Rapid Communications

Anisotropy induced vortex lattice rearrangement in $CaKFe_4As_4$

Rustem Khasanov,[1,*] William R. Meier,[2,3] Sergey L. Bud'ko,[2,3] Hubertus Luetkens,[1] Paul C. Canfield,[2,3] and Alex Amato[1]

[1]*Laboratory for Muon Spin Spectroscopy, Paul Scherrer Institut, CH-5232 Villigen PSI, Switzerland*

[2]*Division of Materials Science and Engineering, Ames Laboratory, Ames, Iowa 50011, USA*

[3]*Department of Physics and Astronomy, Iowa State University, Ames, Iowa 50011, USA*

(Received 6 February 2019; published 19 April 2019)

The magnetic penetration depth anisotropy $\gamma_\lambda = \lambda_c/\lambda_{ab}$ (λ_{ab} and λ_c are the in-plane and the out-of-plane components of the magnetic penetration depth) in a $CaKFe_4As_4$ single crystal sample (the critical temperature $T_c \simeq 35$ K) was studied by means of muon-spin rotation (μSR). γ_λ is almost temperature independent for $T \lesssim 20$ K ($\gamma_\lambda \simeq 1.9$) and it reaches $\simeq$3.0 by approaching T_c. The change of γ_λ induces the corresponding rearrangement of the flux line lattice (FLL), which is clearly detected via enhanced distortions of the FLL μSR response. A comparison of γ_λ with the anisotropy of the upper critical field ($\gamma_{H_{c2}}$) studied by Meier *et al.* [Phys. Rev. B **94**, 064501 (2016)] reveals that γ_λ is systematically higher than $\gamma_{H_{c2}}$ at low temperatures and approaches $\gamma_{H_{c2}}$ for $T \to T_c$. The anisotropic properties of λ are explained by the multigap nature of superconductivity in $CaKFe_4As_4$ and are caused by anisotropic contributions of various bands to the in-plane and the out-of-plane components of the superfluid density.

DOI: 10.1103/PhysRevB.99.140507

In the majority of superconducting compounds discovered so far, the crystal structure, as well as the electronic and phononic band structures, are all far from being isotropic. Anisotropic superconductors are usually treated within the phenomenological anisotropic Ginzburg-Landau (AGL) theory [1,2], which follows from the isotropic Ginzburg-Landau (GL) approach via replacement of the effective mass m^* in the GL free energy functional by an effective mass tensor, with values m_a^*, m_b^*, and m_c^* along the principal a, b, and c axes [3,4]. In the most usual case of uniaxial anisotropy, all anisotropies are incorporated into the single parameter [5],

$$\gamma = \gamma_\lambda \equiv \frac{\lambda_c}{\lambda_{ab}} = \sqrt{\frac{m_c^*}{m_{ab}^*}} = \gamma_{H_{c2}} \equiv \frac{H_{c2}^{\parallel ab}}{H_{c2}^{\parallel c}} = \frac{\xi_{ab}}{\xi_c}. \qquad (1)$$

Here, γ_λ and $\gamma_{H_{c2}}$ are the anisotropy of the magnetic penetration depth (λ) and the upper critical field (H_{c2}), respectively, and ξ is the coherence length. In AGL theory the same effective mass tensor determines the anisotropy of λ and H_{c2}, thus making both γ_λ and $\gamma_{H_{c2}}$ temperature and field independent [6].

Note, however, that the GL theory is strictly valid only for $T \to T_c$. Following Kogan [7], away from T_c, the theoretical approach for calculating H_{c2} (the position of the second-order phase transition in high fields) has little in common with the evaluation of λ, so that the anisotropies γ_λ and $\gamma_{H_{c2}}$ are not the same and can be substantially different. In MgB_2, e.g., both anisotropies approach a common value $\gamma_\lambda = \gamma_{H_{c2}} \simeq 1.75$ at T_c and become $\gamma_\lambda \simeq 1.2$ and $\gamma_{H_{c2}} \simeq 6$ at low temperatures [8–10]. Different T dependencies of γ_λ and $\gamma_{H_{c2}}$ have also been reported for various cuprate and Fe-based superconductors [11–19].

It is worth mentioning here that the change of γ_λ would necessarily lead to a corresponding flux line lattice (FLL) rearrangement. As follows from Fig. 1(a), for the external field B_{ex} applied along the ab plane ($B_{ex} \parallel ab$), the increase of γ_λ shortens the distance between vortices within the ab plane and enhances the intervortex distances in the c direction. The displacement of vortex lines could be quite big. The simple estimate reveals that the increase of γ_λ from 1.0 to 3.0 leads to a decrease/increase of the in-plane/out-of-plane intervortex distances by almost half of the isotropic FLL unit cell [see Fig. 1(a)]. This effect can be studied, e.g., by using techniques visualizing the vortex distribution in superconducting materials, such as small-angle neutron scattering (SANS), tunneling, or magnetic decoration. The important limitation comes, however, from the sample size and morphology. Most of the available good quality single crystals are very thin along the crystallographic c direction, and a good surface preparation (needed for magnetic decoration and tunneling experiments) in $B_{ex} \perp c$ orientation is challenging.

In this Rapid Communication, we report on measurements of the magnetic penetration depth anisotropy $\gamma_\lambda = \lambda_c/\lambda_{ab}$ in a $CaKFe_4As_4$ single crystal sample ($T_c \simeq 35$ K) by means of muon-spin rotation (μSR). A comparison of γ_λ with $\gamma_{H_{c2}}$ studied in Ref. [21] shows that γ_λ is higher than $\gamma_{H_{c2}}$ all the way up to T_c. Only in the narrow region close T_c, $\gamma_\lambda = \gamma_{H_{c2}} \simeq 3.0$ [Fig. 1(b)]. The change of γ_λ with temperature induces the corresponding rearrangement of the flux line order, which was detected via the enhanced distortions of the FLL μSR response. The temperature dependencies of the in-plane and the out-of-plane components of the superfluid density (λ_{ab}^{-2} and λ_c^{-2}) were found to be well described within the two-gap scenario, thus suggesting that the multiple-band nature of superconductivity in $CaKFe_4As_4$ is well pronounced for both c and ab directions.

*rustem.khasanov@psi.ch

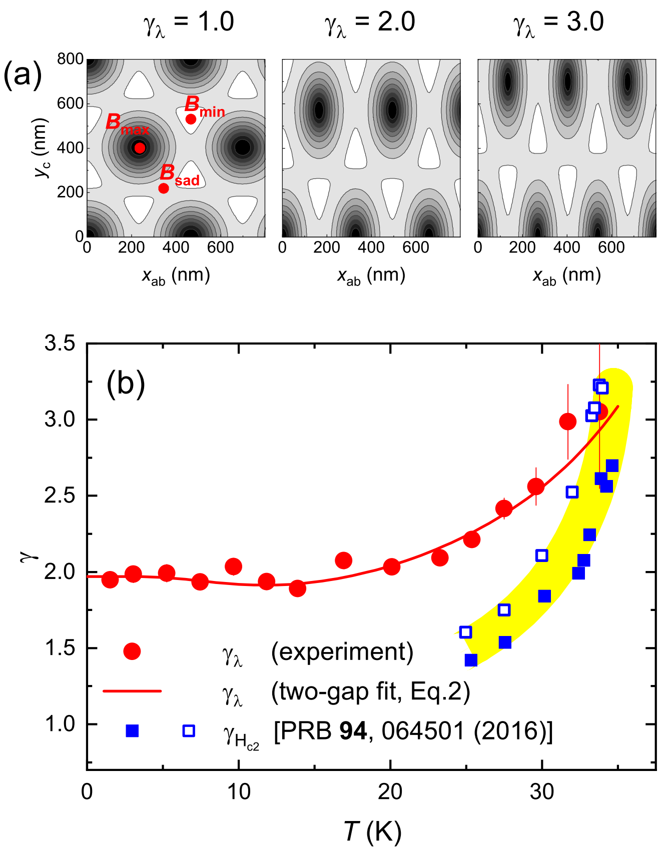

FIG. 1. (a) The contour plot of the field variation within the triangular vortex lattice of an anisotropic superconductor with $B_{ex} \parallel ab$ ($B_{ex} = 11$ mT, $\gamma_\lambda = \lambda_c/\lambda_{ab} = 1.0, 2.0,$ and 3.0; see the Supplemental Material [20]). $B_{\rm min}$, $B_{\rm max}$, and $B_{\rm sad}$ are the minimum, maximum, and the saddle point fields. (b) The anisotropies γ_λ and $\gamma_{H_{c2}}$ of $CaKFe_4As_4$. Solid circles are γ_λ points from the present study. The solid and open squares correspond to $\gamma_{H_{c2}}(T)$ from Ref. [21], as obtained by using the "onset" and "offset" criteria of T_c determination, respectively. The solid red line is the fit of the two-gap model [Eq. (2)] to $\lambda_{ab}^{-2}(T)$ and $\lambda_c^{-2}(T)$ data.

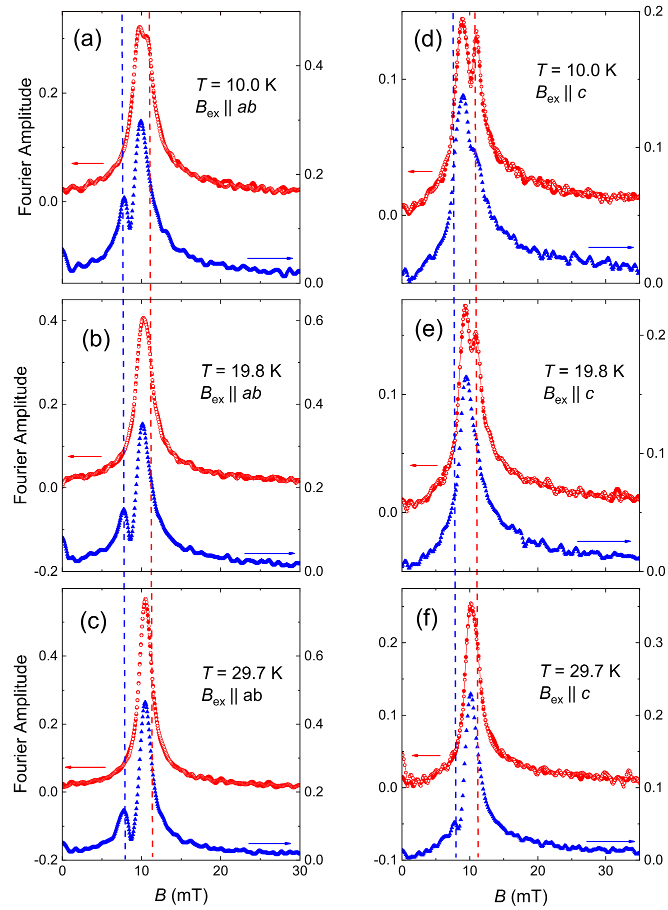

FIG. 2. The fast Fourier transform of the TF-μSR time spectra. (a)–(c) correspond to $B_{ex} \parallel ab$ and (d)–(f) to $B_{ex} \parallel c$ sets of measurements, respectively [27]. The solid and open red symbols are $P(B)$'s obtained by following FCW and FCC protocols at $B_{ex} \simeq 10.8$ mT (see text for details). The blue solid symbols are $P(B)$'s after the field shift down to $\simeq 8$ mT. Dashed lines correspond to the applied field (10.8 mT) and to the "shifted" field (8.0 mT), respectively.

A $CaKFe_4As_4$ single crystal with dimensions of $\simeq 4.0 \times 4.0 \times 0.1$ mm^3 was grown from a high-temperature Fe-As rich melt [21,22], and it is characterized via magnetization measurements (see the Supplemental Material [20]). The μSR measurements were carried out at the πM3 beam line using the GPS spectrometer (Paul Scherrer Institute, Switzerland) [23]. The zero-field (ZF) and transverse-field (TF) μSR measurements were performed at temperatures from $\simeq 1.5$ to 50 K. In two sets of TF-μSR experiments the external magnetic field ($B_{ex} \simeq 10.8$ mT) was applied parallel to the ab plane and the crystallographic c axis of the crystal, respectively. A fraction of the TF-μSR data for $B_{ex} \parallel c$ was previously reported in Ref. [24]. ZF-μSR data are discussed in the Supplemental Material [20]. A special sample holder designed to measure thin samples by means of μSR was used [25]. The experimental data were analyzed using the MUSRFIT package [26].

The homogeneity of the superconducting state in $CaKFe_4As_4$ was checked by performing a series of field-shift experiments. Figure 2 exhibits the fast Fourier transform of the TF-μSR time spectra, which reflects the internal field distribution $P(B)$. Figures 2(a)–2(c) correspond to $B_{ex} \parallel ab$ and Figs. 2(d)–2(f) to $B_{ex} \parallel c$ sets of measurements, respectively. The solid red symbols are $P(B)$'s obtained after cooling the sample at $B_{ex} = 10.8$ mT from a temperature above T_c down to 1.48 K and subsequently warming it up to the measurement temperature [field-cooled warming (FCW) procedure]. The open red symbols are $P(B)$'s obtained after direct cooling from $T > T_c$ to the measurement temperature [field-cooled cooling (FCC) procedure]. The blue solid symbols are $P(B)$ distributions collected by following the FCW protocol and a subsequent decrease of the external field down to $\simeq 8$ mT (field-shift procedure). From the data presented in Fig. 2, the following three important points emerge: (i) The main part of the signal, accounting for approximately 90% of the total signal amplitude, remains unchanged within the experimental error after a field shift. Only the sharp peak ($\simeq 10$% of the signal amplitude) follows exactly the applied field. It is attributed, therefore, to the residual background signal from muons missing the sample (see also Refs. [25,28]). (ii) The asymmetric $P(B)$ distributions shown in Fig. 2 possess the basic features

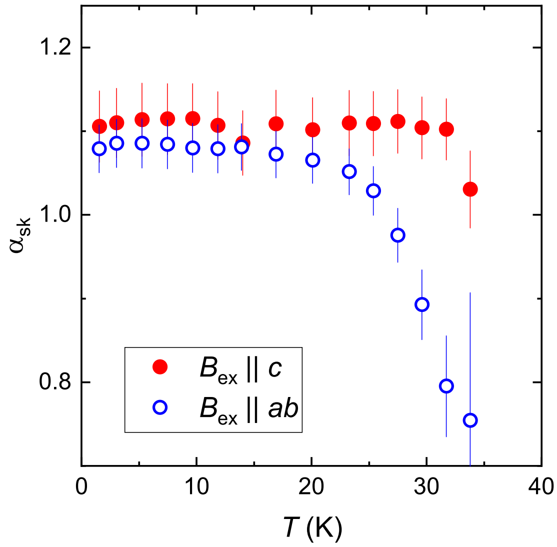

FIG. 3. The temperature dependence of the skewness parameter $\alpha_{sk} = \langle\Delta B^3\rangle^{1/3}/\langle\Delta B^2\rangle_s^{1/2}$ obtained in $B_{ex} \parallel c$ and $B_{ex} \parallel ab$ sets of experiments.

expected for a well aligned vortex lattice, i.e., the cutoff at low fields (B_{min}), the peak arising from the saddle point midway between two adjacent vortices (B_{sad}), and a long tail towards high fields caused by regions around the vortex core (B_{max}) [24,29]. Note that the definition of a "well aligned" FLL is different, e.g., for μSR and SANS experiments. In the μSR case, due to the microscopic nature of the μSR technique, the field at the muon stopping site is determined by the *local* flux line arrangement (within a couple of FLL unit cells). The SANS experiment collects reflections from flux-line planes, which requires a *long-range* arrangement of FLL. Following scanning tunneling microscopy (STM) results, the FLL in $CaKFe_4As_4$ is well arranged on the short length scale, while the long-range arrangement is missing [see Figs. 3(d)–3(f) in Ref. [30]]. (iii) The $P(B)$ curves obtained by following the FCC and FCW protocols coincide for both field orientations and within the full temperature range studied. To conclude, the above experiment demonstrates that the FLL in $CaKFe_4As_4$ sample is well arranged and strongly pinned (at least at $B_{ex} \simeq$ 11 mT). The strong pinning in $CaKFe_4As_4$ was also reported for $B_{ex} \parallel c$ orientation in STM experiments [30], and for both $B_{ex} \parallel ab$ and $B_{ex} \parallel c$ sets of data in magnetization studies [31].

The TF-μSR data were analyzed by fitting a three-component expression to the time evolution of the muon-spin polarization (see the Supplemental Material [20]). The superconducting response of the $CaKFe_4As_4$ sample was further obtained within the framework of the so-called momentum approach, which includes the calculations of the first moment ($\langle B\rangle$), and the second- ($\langle\Delta B^2\rangle$) and third-central moments ($\langle\Delta B^3\rangle$) of the magnetic field distribution function $P(B)$ (see the Supplemental Material [20] for details). Following Ref. [32], the first moment (the mean field) scales with the sample magnetization. The second moment (the broadening of the signal), $\langle\Delta B^2\rangle = \langle\Delta B^2\rangle_s + \sigma_{nm}^2$, contains contributions from the vortex lattice ($\langle\Delta B^2\rangle_s$) and the nuclear dipole field (σ_{nm}, as is obtained from $T > T_c$ measurements). In extreme type-II superconductors ($\lambda \gg \xi$) and for fields $B_{ex} \ll \mu_0 H_{c2}$, $\langle\Delta B^2\rangle_s \propto \lambda^{-4}$ [33,34]. The third moment accounts for the asymmetric shape of $P(B)$, which is described via the skewness parameter $\alpha_{sk} = \langle\Delta B^3\rangle^{1/3}/\langle\Delta B^2\rangle_s^{1/2}$. In the limit of $\lambda \gg \xi$ and for realistic measurement conditions, $\alpha_{sk} \simeq 1.2$, for a well arranged triangular vortex lattice [35]. It is very sensitive to structural changes of the vortex lattice which may occur as a function of temperature and/or magnetic field [35–40].

Figure 3 shows temperature dependencies of the skewness parameter α_{sk} measured in $B_{ex} \parallel c$ ($\alpha_{sk}^{\parallel c}$) and $B_{ex} \parallel ab$ ($\alpha_{sk}^{\parallel ab}$) sets of experiments. The temperature dependencies of the first moment $\langle B\rangle$ and the second-central moment $\langle\Delta B^2\rangle$ are presented in the Supplemental Material [20]. Following Fig. 3, $\alpha_{sk}^{\parallel c}$ stays temperature independent. Only in the close vicinity to T_c, $\alpha_{sk}^{\parallel c}$ decreases by approximately 8% (from $\simeq$1.1 to $\simeq$1.03). This, together with the relatively high value of $\alpha_{sk}^{\parallel c} \simeq$ 1.1, suggests that in $B_{ex} \parallel c$ orientation the FLL in $CaKFe_4As_4$ is well developed and has little distortion. The presence of well arranged FLL is also confirmed in "field-shift" experiments [Figs. 2(d)–2(f)] showing asymmetric $P(B)$'s with all characteristic features attributed to FLL.

The temperature evolution of $\alpha_{sk}^{\parallel ab}$ is, however, different from $\alpha_{sk}^{\parallel c}(T)$ (Fig. 3). By increasing temperature, $\alpha_{sk}^{\parallel ab}$ stays almost constant up to $T \simeq 20$ K ($\alpha_{sk}^{\parallel ab} \simeq 1.07$) and it decreases down to $\simeq$0.7 by approaching T_c. In general, the change of α_{sk} as a function of magnetic field and temperature is associated with the vortex lattice melting [36,37,40], and/or dimensional crossover from a three-dimensional (3D) to a two-dimensional (2D) type of FLL [35,37]. Both processes are thermally activated and caused by increased vortex mobility via loosening the interplanar or intraplanar FLL correlations [37]. In both interpretations, however, the increased vortex mobility leads to decoupling vortices from the pinning centers. This is not the case for $CaKFe_4As_4$ studied here. The field-shift experiments, in $B_{ex} \parallel ab$ orientation, suggest the FLL remains rigid [at least up to $T \simeq 32$ K; see Figs. 2(a)–2(c) and the Supplemental Material [20]]. This, therefore, rather indicates that the decrease of $\alpha_{sk}^{\parallel ab}$ for $T \gtrsim 20$ K is caused by a γ_λ induced rearrangement of the FLL. The change of γ_λ, leading necessarily to the movement of the vortex lines [Fig. 1 (a)], enhances the pinning caused FLL distortions and, as a consequence, reduces the value of the skewness parameter $\alpha_{sk}^{\parallel c}$.

The T dependence of γ_λ was further studied via measurements of the temperature evolutions of the in-plane (λ_{ab}^{-2}) and the out-of-plane (λ_c^{-2}) superfluid density components (Fig. 4). The anisotropy parameter $\gamma_\lambda = \lambda_c/\lambda_{ab}$ is presented in Fig. 1(b). Obviously, γ_λ in $CaKFe_4As_4$ is temperature dependent. It is almost constant ($\gamma_\lambda \simeq 1.9$) for $T \lesssim$ 20 K and increases up to $\simeq$3.0 by approaching T_c. More remarkable is that $\gamma_\lambda(T)$ follows the temperature evolution of the skewness parameter $\alpha_{sk}^{\parallel ab}$. Both $\gamma_\lambda(T)$ and $\alpha_{sk}^{\parallel ab}$ are *constant* for $T \lesssim 20$ K and change almost linearly in the 25 K $\lesssim T < T_c$ region [Figs. 1(b) and 3]. These suggest that the enhancement of FLL distortions, seen via a decrease of $\alpha_{sk}^{\parallel ab}$ (Fig. 3), is caused by the vortex lattice rearrangement [Fig. 1(a)], which, in its turn, is initiated by the temperature dependent anisotropy coefficient γ_λ [Fig. 1(b)].

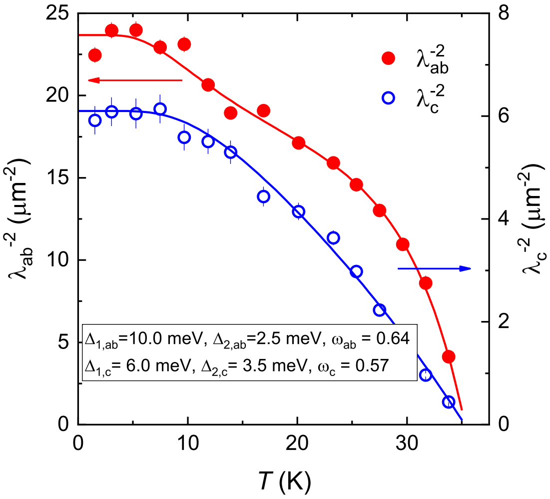

FIG. 4. Temperature dependencies of the inverse squared in-plane (λ_{ab}^{-2}) and the out-of-plane (λ_c^{-2}) components of the magnetic field penetration depth. Solid lines are fits within the framework of the phenomenological α model [12,41].

The comparison of γ_λ obtained in our study with $\gamma_{H_{c2}}$ reported in Ref. [21] shows that these anisotropies coincide with each other ($\gamma_\lambda = \gamma_{H_{c2}} \simeq 3.0$) only for $T \to T_c$ [Fig. 1(b)], thus resembling the situation in the famous two-gap superconductor MgB_2 [8–10]. This may suggest that the range of applicability of AGL to $CaKFe_4As_4$ is confined within a narrow range close to T_c, in full analogy with MgB_2, where the AGL description was found to be limited to temperatures less than 2% away from T_c [42]. An alternative approach, based on microscopic Eilenberger calculations, reveals that in two-gap superconductors (as, e.g., MgB_2) γ_λ and $\gamma_{H_{c2}}$ have different temperature dependencies and cross only at T_c [43]. Which of these approaches better describes the anisotropic properties of $CaKFe_4As_4$ needs further investigation.

The temperature dependencies of λ_{ab}^{-2} and λ_c^{-2} (Fig. 4) were further analyzed within the framework of the phenomenological α model by decomposing $\lambda^{-2}(T)$ into two components [12,41,44],

$$\frac{\lambda^{-2}(T)}{\lambda^{-2}(0)} = \omega\frac{\lambda^{-2}(T,\Delta_1)}{\lambda^{-2}(0,\Delta_1)} + (1-\omega)\frac{\lambda^{-2}(T,\Delta_2)}{\lambda^{-2}(0,\Delta_2)}. \quad (2)$$

Here, $\lambda(0)$ is the value of the penetration depth at $T = 0$, Δ_i is the zero-temperature value of the ith gap ($i = 1$ or 2), and ω ($0 \leqslant \omega \leqslant 1$) is the weight of the larger gap to λ^{-2}. Each component in Eq. (2) was further evaluated by $\lambda^{-2}(T,\Delta)/\lambda^{-2}(0,\Delta) = 1 + 2\int_{\Delta(T)}^{\infty}(\partial f/\partial E)E/\sqrt{E^2-\Delta(T)^2}\,dE$ [5]. Here, $f = [1+\exp(E/k_BT)]^{-1}$ is the Fermi function and $\Delta(T) = \tanh\{1.82[1.018(1/t-1)]^{0.51}\}$ [41]. Note that this equation is valid within the clean limit, which is indeed the case for $CaKFe_4As_4$ [21]. The solid lines in Fig. 4 are fits of Eq. (2) to the $\lambda_{ab}^{-2}(T)$ and $\lambda_c^{-2}(T)$ data. The fit parameters are $\lambda_{ab}^{-2}(0) = 23.4$ (μm^{-2}), $\Delta_{1,ab} = 10.0$ meV, $\Delta_{2,ab} = 2.5$ meV, $\omega_{ab} = 0.64$, and $\lambda_c^{-2}(0) = 6.1$ (μm^{-2}), $\Delta_{1,c} = 6.0$ meV, $\Delta_{2,c} = 3.5$ meV, $\omega_c = 0.57$ for $\lambda_{ab}^{-2}(T)$ and $\lambda_c^{-2}(T)$ data sets, respectively.

From the results of the two-gap model fit to $\lambda_{ab}^{-2}(T)$ and $\lambda_c^{-2}(T)$, three important points emerge: (i) The "theoretical" two-gap $\gamma_\lambda(T)$ curve stays in good agreement with the experimental data [see Fig. 1(b)]. (ii) The density functional theory calculations suggest that in $CaKFe_4As_4$, ten bands (six hole- and four electronlike bands) having different zero-temperature gap values cross the Fermi level [45,46]. Recent angle resolved photoemission spectroscopy (ARPES) [45], as well as the combination of ARPES and μSR experiments [24], confirm this statement. This suggests, on the one hand, that the two-gap approach described by Eq. (2) is oversimplified and contributions of all ten bands need to be included. Such an analysis requires, however, an exact knowledge of the electronic band structure [24,47]. On the other hand, similar two-gap approaches were previously used in Refs. [21,48,49] and allowed to describe satisfactorily the in-plane superfluid density data of $CaKFe_4As_4$. (iii) The differences in the parameters obtained from the two-gap fit to $\lambda_{ab}^{-2}(T)$ and $\lambda_c^{-2}(T)$ are most probably caused by *anisotropic* contributions of various bands to the superfluid density. In such cases Δ_1 and Δ_2 refer to averaged gaps for a series of bands with "big" and "small" gap values, respectively (see, e.g., Ref. [46]), while ω corresponds to the averaged weight of "big" gaps to $\lambda^{-2}(0)$.

To conclude, the magnetic penetration depth anisotropy $\gamma_\lambda = \lambda_c/\lambda_{ab}$ in a $CaKFe_4As_4$ single crystal sample was studied by means of the muon-spin rotation. γ_λ is temperature independent for $T \lesssim 20$ K ($\gamma_\lambda \simeq 1.9$) and it increases up to $\gamma_\lambda \simeq 3.0$ for $T \to T_c$. The change of γ_λ induces the flux line lattice rearrangement, which is clearly detected via the enhanced distortions of the FLL μSR response. The anisotropic properties of λ are explained by the multigap nature of superconductivity in $CKaFe_4As_4$ and caused by anisotropic contributions of various bands to the in-plane and the out-of-plane components of the superfluid density.

The work was performed at the Swiss Muon Source (SμS), Paul Scherrer Institute (PSI, Switzerland). The authors acknowledge helpful discussions with V. G. Kogan. W.R.M. was funded by the Gordon and Betty Moore Foundation EPiQS Initiative through Grant No. GBMF4411. Work at Ames Laboratory was supported by the U.S. Department of Energy, Office of Science, Basic Energy Sciences, Materials Science and Engineering Division. Ames Laboratory is operated for the U.S. DOE by Iowa State University under Contract No. DE-AC02-07CH11358.

[1] V. L. Ginzburg and L. D. Landau, Zh. Eksp. Teor. Fiz. **20**, 1064 (1950).
[2] V. L. Ginzburg, Zh. Eksp. Teor. Fiz. **23**, 236 (1952).
[3] C. Caroli, P. G. de Gennes, and J. Matricon, Phys. Kondens. Mater. **1**, 176 (1963).
[4] S. L. Thiemann, Z. Radović, and V. G. Kogan, Phys. Rev. B **39**, 11406 (1989).

[5] M. Tinkham, *Introduction to Superconductivity* (Krieger, Malabar, FL, 1975).
[6] L. P. Gor'kov and T. K. Melik-Barkhudarov, Sov. Phys. JETP **18**, 1031 (1964).
[7] V. G. Kogan, Phys. Rev. Lett. **89**, 237005 (2002).
[8] M. Angst, R. Puzniak, A. Wisniewski, J. Jun, S. M. Kazakov, J. Karpinski, J. Roos, and H. Keller, Phys. Rev. Lett. **88**, 167004 (2002).
[9] M. Angst and R. Puzniak, in *Focus on Superconductivity*, edited by B. P. Martines (Nova Science, New York, 2004), Vol. 1, pp. 1–49.
[10] J. D. Fletcher, A. Carrington, O. J. Taylor, S. M. Kazakov, and J. Karpinski, Phys. Rev. Lett. **95**, 097005 (2005).
[11] R. Khasanov, A. Shengelaya, A. Bussmann-Holder, J. Karpinski, H. Keller, and K. A. Müller, J. Supercond. Novel Magn. **21**, 81 (2008).
[12] R. Khasanov, S. Strässle, D. Di Castro, T. Masui, S. Miyasaka, S. Tajima, A. Bussmann-Holder, and H. Keller, Phys. Rev. Lett. **99**, 237601 (2007).
[13] R. Prozorov, M. A. Tanatar, R. T. Gordon, C. Martin, H. Kim, V. G. Kogan, N. Ni, M. E. Tillman, S. L. Bud'ko, and P. C. Canfield, Physica C **469**, 582 (2009).
[14] R. Khasanov, D. V. Evtushinsky, A. Amato, H.-H. Klauss, H. Luetkens, C. Niedermayer, B. Büchner, G. L. Sun, C. T. Lin, J. T. Park, D. S. Inosov, and V. Hinkov, Phys. Rev. Lett. **102**, 187005 (2009).
[15] R. Khasanov, A. Maisuradze, H. Maeter, A. Kwadrin, H. Luetkens, A. Amato, W. Schnelle, H. Rosner, A. Leithe-Jasper, and H.-H. Klauss, Phys. Rev. Lett. **103**, 067010 (2009).
[16] S. Weyeneth, R. Puzniak, N. D. Zhigadlo, S. Katrych, Z. Bukowski, J. Karpinski, and H. Keller, J. Supercond. Novel Magn. **22**, 347 (2009).
[17] S. Weyeneth, R. Puzniak, U. Mosele, N. D. Zhigadlo, S. Katrych, Z. Bukowski, J. Karpinski, S. Kohout, J. Roos, and H. Keller, J. Supercond. Novel Magn. **22**, 325 (2009).
[18] M. Bendele, S. Weyeneth, R. Puzniak, A. Maisuradze, E. Pomjakushina, K. Conder, V. Pomjakushin, H. Luetkens, S. Katrych, A. Wisniewski, R. Khasanov, and H. Keller, Phys. Rev. B **81**, 224520 (2010).
[19] S. O. Katterwe, T. Jacobs, A. Maljuk, and V. M. Krasnov, Phys. Rev. B **89**, 214516 (2014).
[20] See Supplemental Material at http://link.aps.org/supplemental/10.1103/PhysRevB.99.140507 for a description of the experimental techniques and the data analysis procedure, which includes Refs. [50–58].
[21] W. R. Meier, T. Kong, U. S. Kaluarachchi, V. Taufour, N. H. Jo, G. Drachuck, A. E. Böhmer, S. M. Saunders, A. Sapkota, A. Kreyssig, M. A. Tanatar, R. Prozorov, A. I. Goldman, F. F. Balakirev, A. Gurevich, S. L. Bud'ko, and P. C. Canfield, Phys. Rev. B **94**, 064501 (2016).
[22] W. R. Meier, T. Kong, S. L. Bud'ko, and P. C. Canfield, Phys. Rev. Mater. **1**, 013401 (2017).
[23] A. Amato, H. Luetkens, K. Sedlak, A. Stoykov, R. Scheuermann, M. Elender, A. Raselli, and D. Graf, Rev. Sci. Instrum. **88**, 093301 (2017).
[24] R. Khasanov, W. R. Meier, Y. Wu, D. Mou, S. L. Bud'ko, I. Eremin, H. Luetkens, A. Kaminski, P. C. Canfield, and A. Amato, Phys. Rev. B **97**, 140503(R) (2018).
[25] R. Khasanov, H. Zhou, A. Amato, Z. Guguchia, E. Morenzoni, X. Dong, G. Zhang, and Z.-X. Zhao, Phys. Rev. B **93**, 224512 (2016).
[26] A. Suter and B. M. Wojek, Phys. Proc. **30**, 69 (2012).
[27] In $B_{\rm ex} \parallel c$ experiments, the external field $B_{\rm ex} = 10.8$ mT is applied perpendicular to the flat surface of the sample. Due to big demagnetization effects in such geometry (the demagnetization factor $N \simeq 0.98$ [59]), the vortex lattice forms at fields higher than $\mu_0 H_{\rm c1}^{\parallel c}(0) \cdot (1 - N) \simeq 0.4$ mT [$\mu_0 H_{\rm c1}^{\parallel c}(0) \simeq 20.8$ mT [20]]. In $B_{\rm ex} \parallel ab$ experiments, $B_{\rm ex} = 10.8$ mT is slightly smaller than $\mu_0 H_{\rm c1}^{\parallel ab}(0) \simeq 12.2$ mT [20]. However, due to the presence of a strong pinning in $CaKFe_4As_4$ [30,31], the "rigid" FLL sets in slightly below T_c, where $B_{\rm ex} \gg \mu_0 H_{\rm c1}^{\parallel ab}(T \simeq T_c) \simeq 0$, and remains unchanged by further cooling down the sample.
[28] J. E. Sonier, R. F. Kiefl, J. H. Brewer, D. A. Bonn, J. F. Carolan, K. H. Chow, P. Dosanjh, W. N. Hardy, R. Liang, W. A. MacFarlane, P. Mendels, G. D. Morris, T. M. Riseman, and J. W. Schneider, Phys. Rev. Lett. **72**, 744 (1994).
[29] A. Maisuradze, R. Khasanov, A. Shengelaya, and H. Keller, J. Phys.: Condens. Matter **21**, 075701 (2009).
[30] A. Fente, W. R. Meier, T. Kong, V. G. Kogan, S. L. Bud'ko, P. C. Canfield, I. Guillamón, and H. Suderow, Phys. Rev. B **97**, 134501 (2018).
[31] S. J. Singh, M. Bristow, W. R. Meier, P. Taylor, S. J. Blundell, P. C. Canfield, and A. I. Coldea, Phys. Rev. Mater. **2**, 074802 (2018).
[32] M. Weber, A. Amato, F. N. Gygax, A. Schenck, H. Maletta, V. N. Duginov, V. G. Grebinnik, A. B. Lazarev, V. G. Olshevsky, V. Y. Pomjakushin, S. N. Shilov, V. A. Zhukov, B. F. Kirillov, A. V. Pirogov, A. N. Ponomarev, V. G. Storchak, S. Kapusta, and J. Bock, Phys. Rev. B **48**, 13022 (1993).
[33] E. H. Brandt, Phys. Rev. B **37**, 2349(R) (1988).
[34] E. H. Brandt, Phys. Rev. B **68**, 054506 (2003).
[35] C. M. Aegerter, J. Hofer, I. M. Savić, H. Keller, S. L. Lee, C. Ager, S. H. Lloyd, and E. M. Forgan, Phys. Rev. B **57**, 1253 (1998).
[36] S. L. Lee, P. Zimmermann, H. Keller, M. Warden, I. M. Savić, R. Schauwecker, D. Zech, R. Cubitt, E. M. Forgan, P. H. Kes, T. W. Li, A. A. Menovsky, and Z. Tarnawski, Phys. Rev. Lett. **71**, 3862 (1993).
[37] T. Blasius, C. Niedermayer, J. L. Tallon, D. M. Pooke, A. Golnik, and C. Bernhard, Phys. Rev. Lett. **82**, 4926 (1999).
[38] G. I. Menon, A. Drew, U. K. Divakar, S. L. Lee, R. Gilardi, J. Mesot, F. Y. Ogrin, D. Charalambous, E. M. Forgan, N. Momono, M. Oda, C. Dewhurst, and C. Baines, Phys. Rev. Lett. **97**, 177004 (2006).
[39] R. Khasanov, T. Kondo, S. Strässle, D. O. G. Heron, A. Kaminski, H. Keller, S. L. Lee, and T. Takeuchi, Phys. Rev. Lett. **101**, 227002 (2008)
[40] D. O. G. Heron, S. J. Ray, S. J. Lister, C. M. Aegerter, H. Keller, P. H. Kes, G. I. Menon, and S. L. Lee, Phys. Rev. Lett. **110**, 107004 (2013).
[41] A. Carrington and F. Manzano, Physica C **385**, 205 (2003).
[42] A. A. Golubov and A. E. Koshelev, Phys. Rev. B **68**, 104503 (2003).
[43] P. Miranović, K. Machida, and V. G. Kogan, J. Phys. Soc. Jpn. **72**, 221 (2003).

[44] H. Padamsee, J. E. Neighbor, and C. A. Shiffman, J. Low Temp. Phys. **12**, 387 (1973).

[45] D. Mou, T. Kong, W. R. Meier, F. Lochner, L.-L. Wang, Q. Lin, Y. Wu, S. L. Bud'ko, I. Eremin, D. D. Johnson, P. C. Canfield, and A. Kaminski, Phys. Rev. Lett. **117**, 277001 (2016).

[46] F. Lochner, F. Ahn, T. Hickel, and I. Eremin, Phys. Rev. B **96**, 094521 (2017).

[47] D. V. Evtushinsky, D. S. Inosov, V. B. Zabolotnyy, M. S. Viazovska, R. Khasanov, A. Amato, H.-H. Klauss, H. Luetkens, C. Niedermayer, G. L. Sun, V. Hinkov, C. T. Lin, A. Varykhalov, A. Koitzsch, M. Knupfer, B. Büchner, A. A. Kordyuk, and S. V. Borisenko, New J. Phys. **11**, 055069 (2009).

[48] K. Cho, A. Fente, S. Teknowijoyo, M. A. Tanatar, K. R. Joshi, N. M. Nusran, T. Kong, W. R. Meier, U. Kaluarachchi, I. Guillamón, H. Suderow, S. L. Bud'ko, P. C. Canfield, and R. Prozorov, Phys. Rev. B **95**, 100502(R) (2017).

[49] P. K. Biswas, A. Iyo, Y. Yoshida, H. Eisaki, K. Kawashima, and A. D. Hillier, Phys. Rev. B **95**, 140505(R) (2017).

[50] J. E. Sonier, K. F. Poon, G. M. Luke, P. Kyriakou, R. I. Miller, R. Liang, C. R. Wiebe, P. Fournier, and R. L. Greene, Phys. Rev. Lett. **91**, 147002 (2003).

[51] R. Khasanov, K. Conder, E. Pomjakushina, A. Amato, C. Baines, Z. Bukowski, J. Karpinski, S. Katrych, H.-H. Klauss, H. Luetkens, A. Shengelaya, and N. D. Zhigadlo, Phys. Rev. B **78**, 220510(R) (2008).

[52] R. Khasanov, H. Luetkens, A. Amato, H.-H. Klauss, Z.-A. Ren, J. Yang, W. Lu, and Z.-X. Zhao, Phys. Rev. B **78**, 092506 (2008).

[53] R. Khasanov, D. G. Eshchenko, D. Di Castro, A. Shengelaya, F. La Mattina, A. Maisuradze, C. Baines, H. Luetkens, J. Karpinski, S. M. Kazakov, and H. Keller, Phys. Rev. B **72**, 104504 (2005).

[54] A. Yaouanc, P. Dalmas de Réotier, and E. H. Brandt, Phys. Rev. B **55**, 11107 (1997).

[55] E. H. Brandt, J. Low Temp. Phys. **26**, 709 (1977).

[56] E. H. Brandt, J. Low Temp. Phys. **73**, 355 (1988).

[57] J. Rammer, Physica C **177**, 421 (1991).

[58] T. M. Riseman, J. H. Brewer, K. H. Chow, W. N. Hardy, R. F. Kiefl, S. R. Kreitzman, R. Liang, W. A. MacFarlane, P. Mendels, G. D. Morris, J. Rammer, J. W. Schneider, C. Niedermayer, and S. L. Lee, Phys. Rev. B **52**, 10569 (1995).

[59] R. Prozorov and V. G. Kogan, Phys. Rev. Appl. **10**, 014030 (2018).